Int. J. Electrochem. Sci., 6 **(2011)** 5228 - 5248

International Journal of
ELECTROCHEMICAL
SCIENCE
www.electrochemsci.org

Preparation and Corrosion Performance of PEO Coating With Low Porosity on Magnesium Alloy AZ91D In Acidic KF System

Wei Zhang[1,*], *Bo Tian*[2], *Ke-Qin Du*[1], *Hui-Xia Zhang*[3], *Fu-Hui Wang*[1]

[1] State Key Laboratory for Corrosion and Protection, Institute of Metal Research, Chinese Academy of Sciences, 62 Wencui Road, Shenyang 110016, China
[2] School of Science, Shenyang University of Technology, 111 Shenliao West Road, Shenyang 110178, China
[3] Science and Technology on Marine Corrosion and Protection Laboratory, Luoyang Ship Material Research Institute, 149-1 Zhuzhou Road, Qingdao 266101, China
[*]E-mail: weizhang@imr.ac.cn

Received: 1 September 2011 / *Accepted:* 2 October 2011 / *Published:* 1 November 2011

A plasma electrolytic oxidation (PEO) ceramic coating F-B-A with excellent compactness was prepared on magnesium alloy AZ91D in acidic KF solution with dihydric phosphate by applying a bi-polar pulse voltage. For comparison, two other coatings F-M and F-M-A were prepared in the same solution with and without addition of dihydric phosphate by applying a mono-polar pulse voltage. The composition and microstructure of the coatings were characterized by XRD, XPS and SEM. While their corrosion performance in 3.5% NaCl solution was examined by potentiodynamic polarization and electrochemical impedance spectroscopy (EIS). Results showed that the F-B-A coating was uniform and compact without fissures on surface, and its porosity was around 4.8%; while the other coatings were loose and porous with porosity around 45.6% and 27.9%, respectively. The F-B-A coating showed a bi-layered microstructure, of which the outer consisted mainly of $KMgF_3$ and MgF_2 with seldom MgO, whereas, the inner mainly of MgF_2, Mg_3 $(PO4)_2$, $MgHPO_4$ and little MgO. The magnesium alloy with F-B-A coating exhibited corrosion resistance about three orders higher than the sample with the F-M coating. EIS tests indicated that this bi-layered coating slowed down the penetration rate of chlorine ions and postponed the initiation of pitting corrosion on substrate.

Keywords: PEO coating; magnesium alloy; KF based electrolyte; bipolar mode; corrosion behavior

1. INTRODUCTION

Corrosion, particularly galvanic corrosion, is a complicated and serious problem in applications of Mg and its alloys [1]. To improve the corrosion resistance, many surface modification techniques have been applied to Mg alloys, such as electrochemical plating, conversion coating, anodizing and plasma electrolysis oxidation (PEO) [2-3]. Among these techniques, PEO, as a relatively new and

effective surface treatment technique derived from the conventional anodic oxidation, has been widely investigated and used to apply ceramic coatings on Mg alloys. After PEO process, the wear resistance, corrosion resistance, mechanical strength and electrical insulation of Mg alloys can be greatly enhanced [3-5].

In general, the microstructure of PEO coating is composed of an outer porous layer and an inner barrier layer. Some literatures report the composition and quality of the inner barrier layer has a considerable influence on the corrosion resistance of the coating [6]. While the resistance of the outer porous layer of PEO coating is too weak in comparison to that of the compact barrier layer, thus it does not contribute significantly to the corrosion protection of Mg substrate [7]. In fact, since micro pores of various sizes always existed and distributed uniformly inside the porous outer layer of PEO coatings. These micro pores, acting as transportation passage for the corrosive ions, thereby, corrosive media may rapidly enter onto the barrier layer of PEO coating and so that decrease largely the protectiveness of the PEO coatings [4,5]. It is believed that a preparation process can produce a good quality of inner barrier layer, and simultaneously, lower the porosity of the porous layer should be helpful to upgrade the corrosion performance of PEO coatings.

The structures of PEO coating on Mg alloy depend on processing parameters, such as chemical composition of electrolyte, electric parameters, alloy composition of substrate, pretreatment and post treatment etc. Especially, the chemical composition of the electrolyte exerts a considerable influence on the formation and property of effective oxide layer for Mg alloy [7-8]. Therefore, it is significant to select proper base electrolyte compositions to improve the compactness and its corrosion resistance on Mg alloys of PEO coating.

Recently many studies concerned with corrosion performance of Mg alloys coated with PEO coatings, and much attention has been paid on the effect of electrolyte composition on the performance of PEO coatings. Among these studies, weak alkaline electrolyte such as silicate and phosphate systems are usually used as base electrolytes, and many additives, such as F^- and AlO^{2-} containing compounds, are adopted to improve the property of PEO coating. Results show that F− containing compounds are the promising additives for PEO process [3, 8-10]. Addition of F− helps to form the stable products MgF_2, which can reduce the anodic dissolution of the Mg alloy substrate and also favor the growth of PEO films [11, 12]. Wang et al. indicated that PEO coatings formed in a bath with higher KF showed better corrosion resistance and lower pitting-corrosion tendency [13]. However, in that study F^- containing compounds are the only additives for PEO electrolytes. Presently there is little information in literatures concerning fluoride based electrolytes for preparation of PEO coating on Mg alloy.

Therefore, it is worth to try to use a bath with base electrolyte consisted of KF and tartaric acid to prepare PEO coatings on Mg alloys and then to characterize the nature and corrosion performance of the coatings. It was reported that PEO coatings produced in phosphate based electrolyte were thicker than that in silicate based ones [3, 14-15]. So, phosphate was chosen as an additive for this study. Moreover, the different power supply mode during PEO process will affect the character of spark-discharges occurred on the sample [16, 17], and the microstructure, growth rate, corrosion performance of oxide coating may be improved by bi-polar power supply mode [18]. Thus, the power

supply mode should be considered as an important technical issue for preparing compact PEO coating in this study.

This paper aims to prepare the bi-layered PEO coating with better compactness on Mg alloys. For that purpose a new bath of acidic KF system was employed with peculiar technical parameters such as electrolyte constitutes and power supply mode. Then the morphology and composition of the coatings prepared by various processing parameters were examined by surface analysis techniques, such as SEM, XPS and XRD. Porosity of PEO coatings was calculated by image analysis and electrochemical methods. Potentiodynamic polarization and electrochemical impedance spectroscopy (EIS) were used to study the corrosion behavior of the compact PEO coating in 3.5% NaCl solution for short-term and long-term.

2. EXPERIMENTAL PROCEDURES

2.1 Preparation of PEO coatings

Rectangular samples (30mm×60mm×15mm) of magnesium alloy AZ91D (Al 8.5–9.5%, Zn 0.50–0.90%, Mn 0.17–0.27% and Mg balance) were used as the working electrodes. Prior to PEO treatment, the samples were successively grounded with a series of SiC abrasive papers (up to 1000 grid), then cleaned in detergent and distilled water.

The plasma electrolytic oxidation (PEO) processes were carried out in acidic KF based electrolytes with and without dihydric phosphate. Besides, mono-polar pulse voltage and bi-polar pulse voltage were used; their waveforms were shown in Fig.1. By the mono-polar pulse voltage, PEO coatings prepared in acidic KF electrolyte, without and with additives, respectively were named as F-M and F-M-A. While the PEO coating prepared in acidic KF electrolyte with additives by using the bi-polar pulse voltage, was known as F-B-A. The main pulse parameters, such as pulse duration, voltage amplitude and duty cycle during both positive and negative bias can be adjusted independently. In experiments, the electrical parameters were fixed as follows: frequency 500Hz, the positive pulse 2.0ms, the negative pulse 1.2ms, and duty cycle 50 %(+): 30 %(-). It should be noticed that by the bi-polar pulse voltage, the starting time of negative pulse voltage was later than that of the positive pulse voltage. This moment, an integrated anodized dielectric film was formed on the surface of Mg substrate.

During PEO process, the AZ91D magnesium samples and the graphite electrode were used as the anode and the counter electrode respectively. The voltage was 400~500V in the positive pulse cycle and 50~100V in the negative pulse cycle. The constant current density 2 A/dm^2 was maintained by controlling the voltage. The temperature of the electrolyte was kept below 50℃ by a water cooling system. After PEO treatment, the coated samples were rinsed thoroughly in water and dried in warm air. Detailed description of the electrolytes and process parameters used for deposition of PEO coatings were given in Table 1.

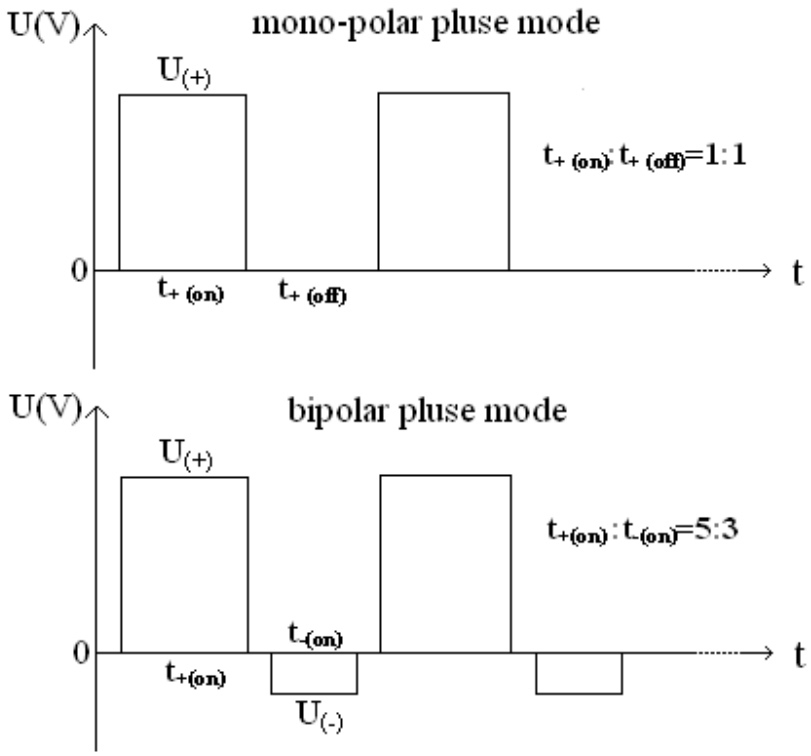

Figure 1. Typical diagrams of the output voltage signals of the pulse DC power supply (a) mono-polar pulse mode; (b) bi-polar pulse mode

Table 1. Experimental condition for preparation of PEO coatings on magnesium alloy AZ91D

Sample code	Electrolyte composition	Treatment time	Current density	Frequency	Terminal voltage and Power supply model	pH
F-M	15g/lKF+2g/l tartaric acid	60min	2A/cm^{-2}	500Hz	~500V(+) mono-polar pulse	~6.2
F-M-A	15g/lKF+2g/l tartaric acid+ 3~5g/lKH_2PO_4	60min	2A/cm^{-2}	500Hz	~470V(+) mono-polar pulse	~5.8
F-B-A	15g/lKF+2g/l tartaric acid+ 3~5g/lKH_2PO_4	60min	2A/cm^{-2}	500Hz	~420V(+); ~60V(-) bipolar pulse	~5.8

2.2 The microstructure and composition of PEO coatings

The phase constituents of the PEO ceramic coatings were characterized by X-ray diffraction (XRD, PHILIPS, PW1700) using a CuKα radiation under 40kV voltage. Surface morphology and cross-sectional image of the coatings were observed using a scanning electron microscope (SEM, PHILIPS, XL-30FEG). In order to prevent surface charging effects, the oxide films were sputtered with a thin gold film. XPS (ESCALAB 250 VG Company Model) was applied to determine the

chemical states of elements in the PEO coating. The binding energy was calibrated with the C1s core level peak at 285.6 eV.

2.3 Porosity measurement

Direct and indirect methods were combined to represent the porosity of PEO coatings on the AZ91D magnesium. Firstly, Image analysis method was carried out to quantify the porosity level [19, 20]. SEM images were analyzed using Image 1.62 software from NIH. Pores and cracks in the coating were isolated implementing several filtering protocols. The porosity level was the sum of the pores relative areas, A_P and the cracks cumulated areas, A_V. As the tiny pore or crack in inner barrier layer of PEO coating was too small to be described by the image analysis, the porosity level acquired by this method tended to reflect the porosity of the outer portion of PEO coating.

The electrochemical method is an effective means to determine through-coating porosity. Liu et al. [21] proposed an empirical equation to estimate the conductive porosity (F) of the coating. This equation is a complemented equation of porosity measurement suggested by Matthews and co-workers [22]; the determination of the total coating porosity (F) is possible according to Eq. (2):

$$F = \frac{R_{pm(substrate)}}{R_{p(coating-substrate)}} \times 10^{-|\Delta Ecorr/\beta a|} \times 100\% \qquad (2)$$

Where F is the total coating porosity, R_{pm} the polarization resistance of the substrate, R_p the polarization resistance of the coating/magnesium system. ΔE_{corr} is the difference of corrosion potentials between the coating and the substrate, and β_a the anodic Tafel slope of the substrate. Usually the corrosive media corroded substrate by passing-through the opening pore of PEO coating, especially, the micro-pores or cracks in the barrier layer; therefore, through-coating porosity can partly judge the quality of the barrier layer of PEO coating.

2.4 Electrochemical tests

Electrochemical properties of the coatings formed on magnesium alloy AZ91D were investigated using a Princeton Applied Research (PAR) EG&G potentiostat/galvanostat model 273 and EG&G 5210 lock-in amplifier with computer interface. A conventional three electrodes electrochemical cell was employed, the coated and uncoated magnesium alloy AZ91D samples was used as working electrode, a platinum plate as auxiliary electrode and a saturated calomel electrode (SCE) as reference. The measurements were carried out in 3.5% NaCl solution at ambient temperatures, and the solution was aerated with purified nitrogen gas in order to eliminate the interference of dissolved oxygen. The exposed sample surface area was 1.54 cm^2. For measuring the porosity of PEO coating, before the polarization, the sample was immersed in 3.5% NaCl solution for 10 hours.

Potentiodynamic polarization tests were carried out at a scan rate of 0.2mV/s from -0.25V versus open circuit potential (OCP) to a certain positive potential at which the clear pitting corrosion was observed on the samples. The impedance measurements were carried out at open circuit potential (OCP), a 5 mV sine-wave perturbation signal and a frequency range from 0.01 Hz to 0.1 MHz were used. The polarization and impedance data were fitting by the analysis software CorrView2 and ZView2

3. RESULTS AND DISCUSSIONS

3.1 Morphology observation of PEO coatings

Surface and cross-sectional morphologies of PEO coatings prepared in acidic KF based electrolytes, without and with dihydric phosphate, with different processing parameters were illustrated in Fig. 2. From Fig. 2(a) and (b), it can be seen that the morphology of F-M coating was similar to that of F-M-A coating. Both of them had many micro pores and some micro cracks on the surfaces. Great deals of ceramic particles randomly scattered in the coating due to plasma-sparks sintering effect during PEO process. However, close examination of the two coatings revealed that F-M-A coating was much denser with smaller ceramic particles than F-M coating. As addition of dihydric phosphate into the KF solution, the terminal oxidation voltage applied on the anode's surface have decreased (Table 1), which can reduce the size of plasma sparks produced on the sample, therefore, the sintered ceramic particles formed in the F-M-A coating will become thinner[23]. For the morphology of F-B-A coating obtained in the KF electrolyte containing dihydric phosphate by bi-polar pulse electrical mode(Fig.2(c)), its surface presented an integrated compact appearance without any single scattered ceramic particles, only a little pores with the size range from 1μm to 5μm distributed homogeneously in the coating. It is because that bi-polar pulse model can increase the micro-channel numbers produced by the spark discharge and improve the rate of plasma-discharge in the oxide film and hence the hot-chemical synthesis reaction coming from the plasma-spark produced into the coating will be aggravated correspondingly[16, 24]. Thus, by the stronger spark-discharge effect, the original single scatter ceramic particles produced in the coating may be re-melted, fully sintered and solidified to be an integral structure. This process makes the PEO coating much more compact.

From the cross-sectional morphologies of the three PEO coatings on Mg alloy AZ91D shown in Fig. 2, it can be seen that F-M coating (Fig.2 (d)) exhibited a single loose porous structure, and there were lot of obvious cracks and big pores distributed in it. Furthermore, many cracks and pores were also observed near the interface between the substrate and the coating, which may weaken the adhesive strength of ceramic coating to the substrate and reduced the corrosion resistance of PEO coating. In case of F-M-A coating produced in the KF based solution with dihydric phosphate (Fig.2 (e)), there were some macro pores distributed on the outer layer of PEO coating. However, in the inner barrier layer of PEO coating, only small micro pore and crack was observed, moreover, the whole layer was obviously thicker than that of F-M coating. Obviously, the KF based electrolyte with phosphate additive had a higher reactivity with Mg substrate and provided a relative higher growth rate for the

coating rather than the blank KF electrolyte [10].As shown in Fig.2 (f), F-B-A coating was firmly adhered to the Mg alloy AZ91D substrate. There were only a few tiny pores and tiny cracks distributed in the outer layer of coating. Furthermore, there existed a compact barrier layer of about 1~2μm without any clear pores at the interface between the coating and the substrate. The cross-sectional image of PEO coatings were analyzed with Image 1.62 software, the obtained porosity level was as follows: 45.6% for F-M, 27.9% for F-M-A and 4.8% for F-B-A, respectively. This result indicated that with addition of dihydric phosphate into acidic KF system and by the bi-polar pulse voltage, the outer layer of PEO coating prepared on Mg alloy was gradually densified and eventually showed low porosity.

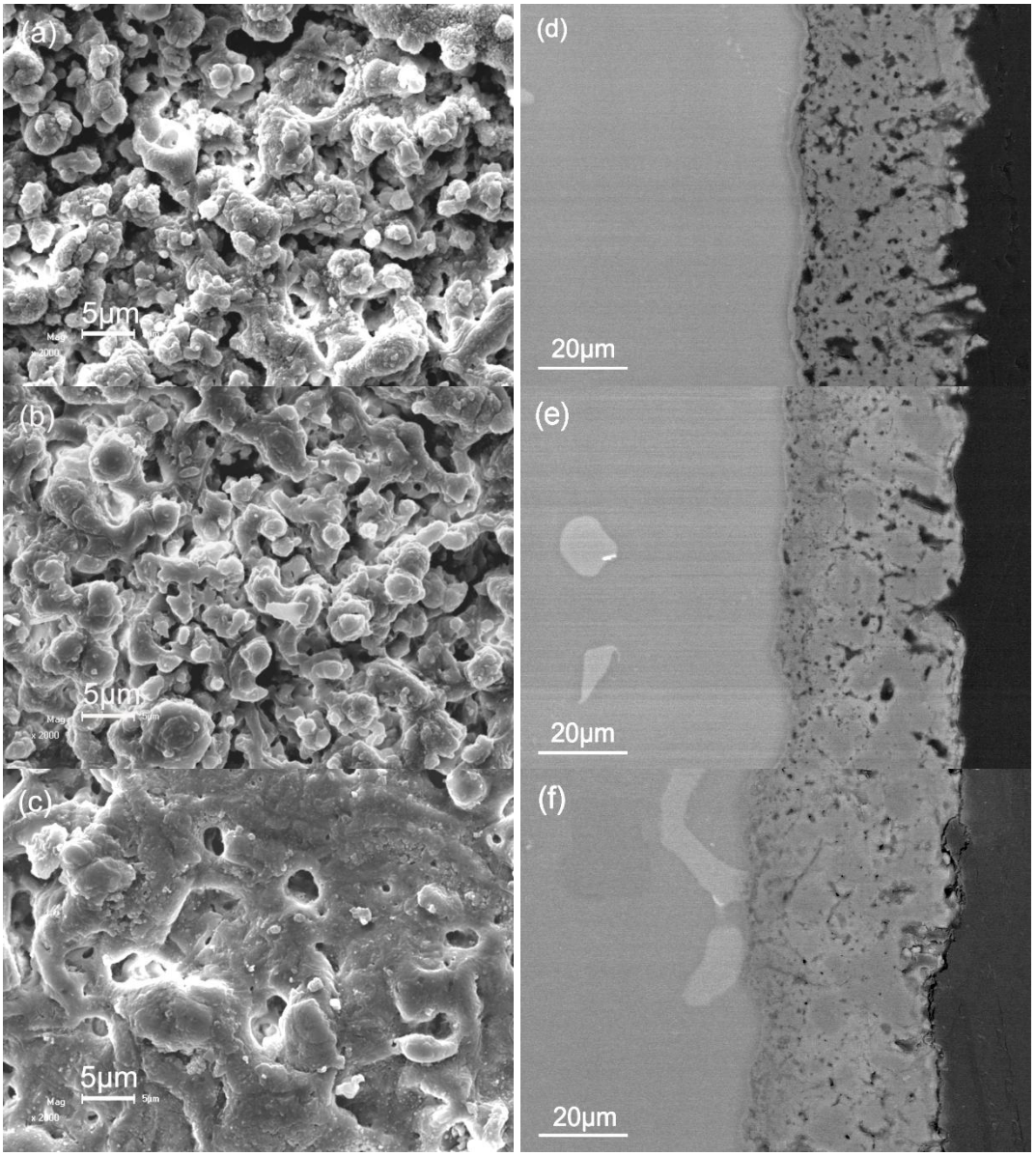

Figure 2. Morphologies of PEO coatings on Mg alloy AZ91D respectively, F-M coating (a), F-M-A coating (b) and F-B-A coating (c) are their surface morphologies; (d), (e) and (f) are their corresponding cross-section morphologies.

3.2 Phase analysis of PEO coatings produced in acidic KF system

Fig.3 illustrated the XRD spectra of PEO coatings prepared by varied technical parameters. It showed that the electrolyte composition and pulse electrical mode had an influence on the phase constitute of PEO coatings. As shown in the Fig.3, three PEO coatings were all composed of MgO, MgF_2 and $KMgF_3$, however, the PEO coating prepared from acidic KF electrolyte by mono-pulse voltage was consisted predominantly of MgO, while the PEO coating formed in acidic KF electrolyte with dihydric phosphate and by bi-polar pulse voltage, was consisted with MgF_2 and $KMgF_3$, which might be ascribed to the cathode effect of the negative biasing under the bi-polar pulse mode [25], which then in turn attract more H^+ with positive charge by Coulomb's force into defects and therewith gradually dissolved unstable MgO in the coating. Furthermore, additive of $H_2PO_4^{2-}$ in KF based electrolyte may easily combine with Mg^{2+} and OH^- to form stable phosphate magnesium on Mg alloy [14-15] and hence the formation of unstable MgO phase in the PEO coating might be restricted. It was reported [11-12] that MgF_2 was more stable than MgO because of the lower solubility of MgF_2 in the corrosive solution. Consequently, among the three PEO coatings, the F-B-A coating containing higher fraction of MgF_2 and $KMgF_3$ should possess higher chemical stability.

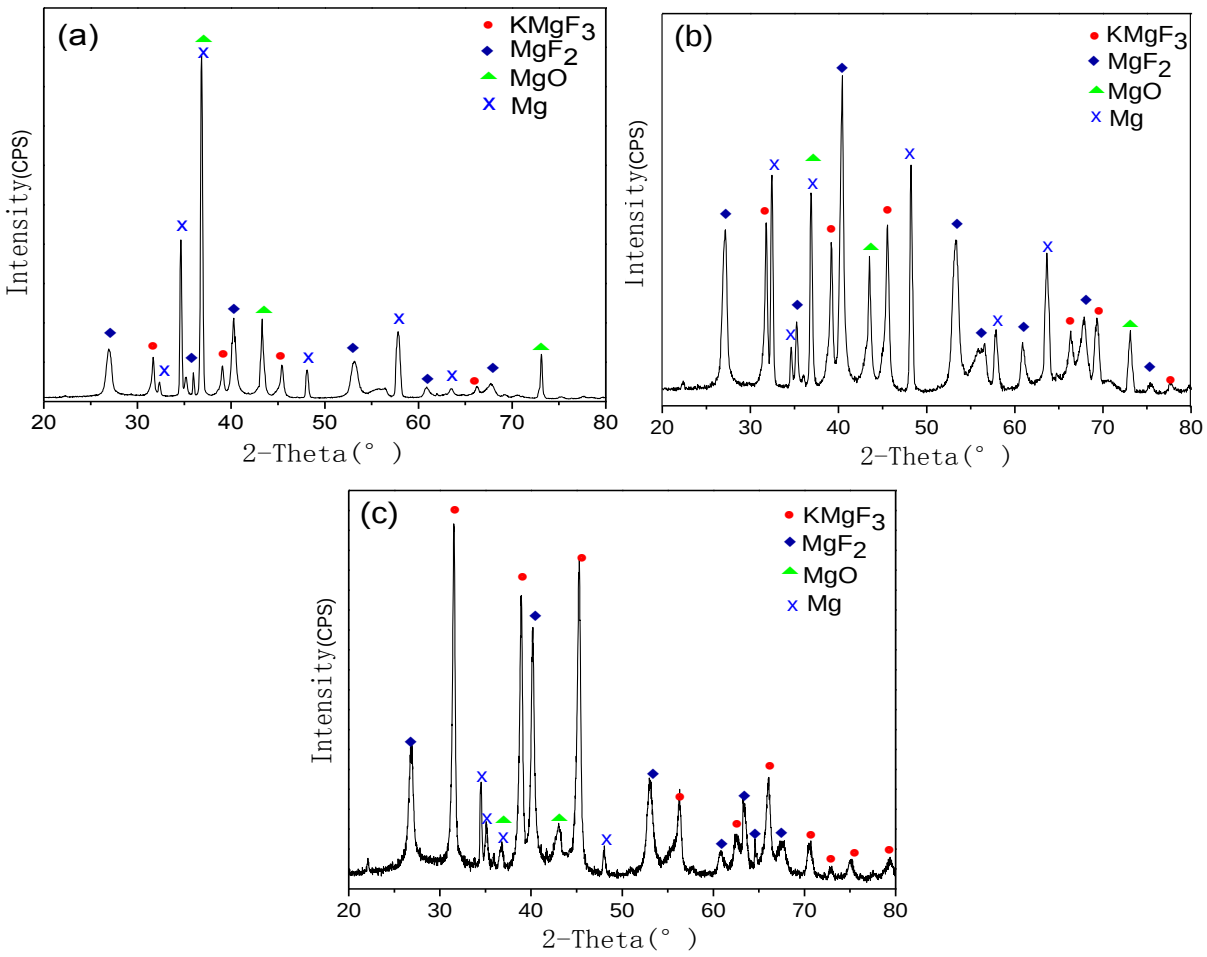

Figure 3. XRD spectra of (a) F-M coating; (b) F-M-A coating; (c) F-B-A coating.

3.2 Chemical compositions of PEO coatings produced in KF electrolyte

The stability and quality of the inner barrier layer of the PEO coating may directly affect its corrosion resistance, which is related with its chemical composition [6], therefore, the compositions of the inner barrier layer of three PEO coatings were studied by XPS analysis, for this purpose the coatings were mechanically thinned up to certain depth so that to let a thickness of around 1 μm of the inner portion of the coating was left.

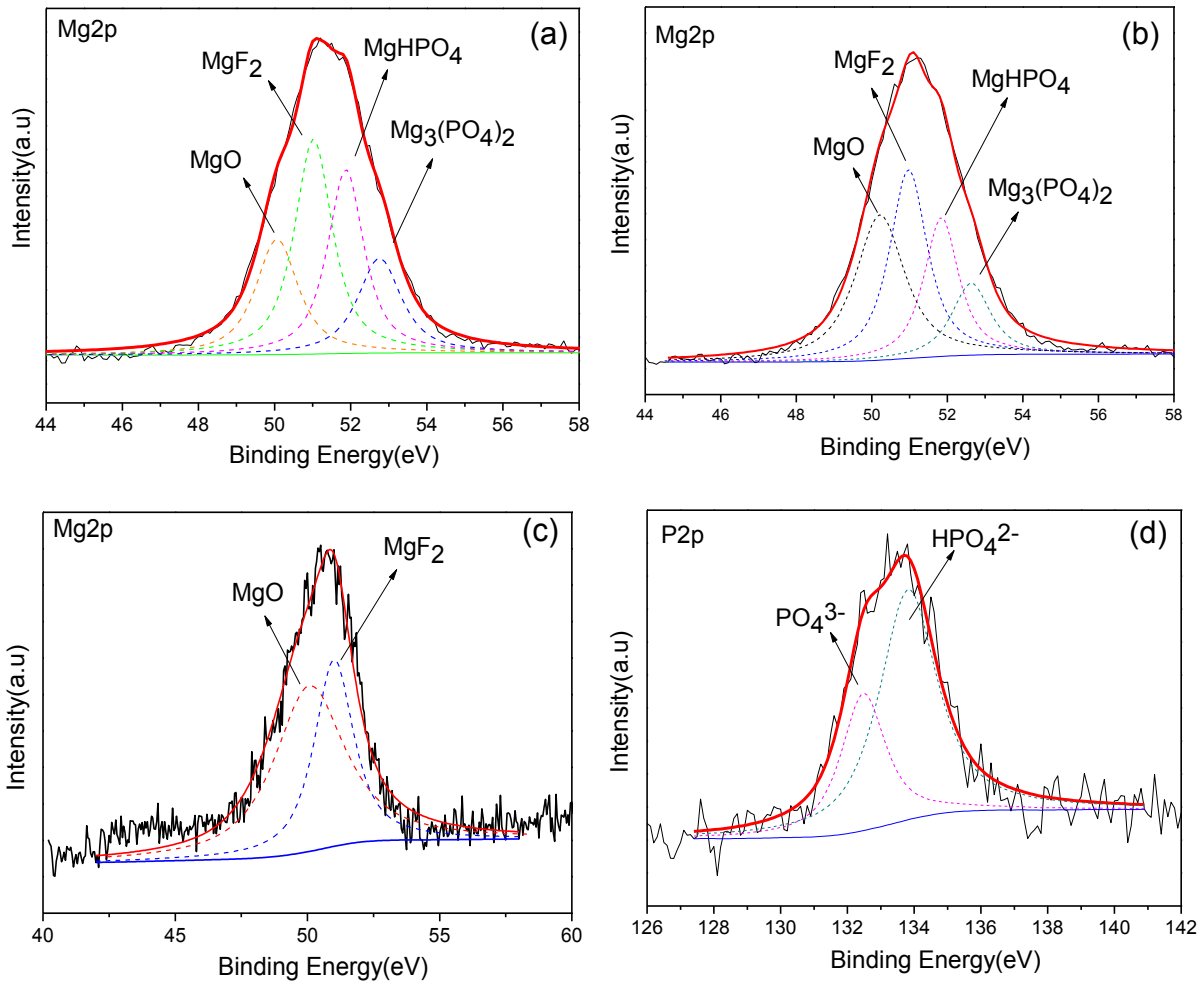

Figure 4. Mg2p spectra of F-B-A (a), F-M-A (b) and F-M (c) and P2p spectra of F-B-A (d)

Fig.4 (a) ~ (b) showed the Mg2p XPS spectra of the inner portions of the F-B-A coating and the F-M-A coating after Ar+ sputtering for 120s. It is clear that from the spectra there existed four compounds, besides MgO (50.15eV) [27] and MgF_2 (50.95eV) [26], the peak Mg2p at 52.65~6.72eV may be well corresponding to Mg_3 $(PO4)_2$ and the peak at 51.86~51.89 eV to $MgHPO_4$ [28, 29]. While the XPS spectra for Mg2p taken from the F-M coating prepared in electrolyte without additives was shown in Fig.4(c). De-convolution analysis of the XPS spectra showed that the binding energy at 50.15eV corresponded to MgO [27], while that at 50.95eV to MgF_2 [26]. Obviously, the new stable

Mg_3 $(PO4)_2$ and $MgHPO_4$ compounds were formed in the inner barrier layer of the F-B-A and F-M-A coating after adding dihydric phosphate into the base electrolyte. For confirming this conclusion, also, Fig. 4(d) demonstrated the deconvolution of the spectra of P2p in the F-B-A coating, clearly, two compounds may be differentiated: the highest peaks 132.4 eV and 133.7 eV represent, respectively, the P-O bonding energies of PO_4^{3-} and HPO_4^{2-} [30]. Making comparative examination of Mg2p spectra of the three PEO coatings, it was found that the peaks area of the compounds MgF_2, Mg_3 $(PO4)_2$ and $MgHPO_4$ for F-B-A coating was all larger than the corresponding ones for the F-M-A and F-M coatings. While the area of peak representing MgO of F-B-A coating was the smallest among the three coatings. Duan et al. [10] have reported that fluoride and phosphate was effective agent in enhancing the corrosion resistance of the inner barrier layer of PEO films. Therefore, a higher fraction of MgF_2, Mg_3 $(PO4)_2$ and MgHPO4 compounds existed in the inner barrier layer of the F-B-A coating may be responsible to its higher stability and better protectiveness.

3.4 Potentiodynamic polarization

The potentiodynamic polarization plots of the magnesium alloy AZ91D with three PEO coatings measured in 3.5% NaCl solution after 10 h immersion, respectively, were shown in Fig.5. For comparison, this figure also shows the curve for the bare magnesium alloy. The relevant electrochemical parameters (E_{corr}, $i_{corr,}$ R_p and β_a) of each sample were calculated and listed in Table 2. It clearly showed that the corrosion resistance of the Mg alloy was greatly improved by the PEO process. In comparison with the corrosion potential of Mg alloy, the corrosion potential of the F-B-A coating was shifted positively 220mV, while only a little shift e.g. ca. 90mV and 30 mV, respectively for the coatings F-M-A and F-M, which again should be attributed to the higher fraction of stable MgF_2 and $KMgF_3$ phases formed in F-B-A coating. The polarization curve of the alloy with F-M coating showed an active dissolution behavior, which was similar with that of the bare alloy. However, the polarization curve of the alloy with F-M-A and F-B-A coatings exhibited passive behavior, the passive region of the alloy with F-B-A coating even reached to ca. 500 mV. Moreover, it can be clearly seen that corrosion current density of the alloy with F-B-A coating was, 1.2969E-9 A/cm^2, two and three orders of magnitude lower than those of F-M-A and F-M coatings, respectively. These results indicated that F-B-A coating possessed the best corrosion resistance in 3.5% NaCl solution among the three coating/alloy systems.

As the main corrosion form of magnesium alloy is pitting corrosion in NaCl solution, the corrosion resistance of coatings may be referred to the blocking effect on the transfer of Cl^- , which then should be directly related with the microstructure of coatings [11, 31]. As shown in Fig.2, F-M coating had only a single porous layer with high porosity 45.6 %. Corrosive Cl^- ions could easily migrate along the opening pore of the coating and arrived rapidly at the interface of the coating/matrix to induce corrosion of the substrate alloy. Thereby, almost no character of passivation was observed in polarization curve (Fig.5). As to the F-M-A coating, although the outer layer of coating was loose and porous, a denser inner barrier layer composed of MgF_2, $MgHPO_4$, Mg_3 $(PO4)_2$ and a little MgO existed in adjacent to the substrate, which could act as an effective protective layer, limiting the transfer rate of

Cl^- to the substrate. Consequently, F-M-A coating exhibited a better passive behavior and a lower corrosion rate rather than F-M coating. In the contrast, the F-B-A ceramic film consisted of a much compact outer layer, especially, and a nearly pore free inner barrier layer (Fig.2), hence, the F-B-A coating will suppress greatly the chloride-induced corrosion on the substrate material. Besides, the inner barrier layer with higher proportion of stable MgF_2, $MgHPO_4$ and Mg_3 $(PO4)_2$ could be helpful maintain longer period of passive behavior of the coating. Therefore, excellent corrosion resistance of the F-B-A coating may imply the important role played by both of the phosphate addition in KF based electrolyte and the application of bipolar pulse mode during preparation of PEO coating on Mg alloy AZ91D.

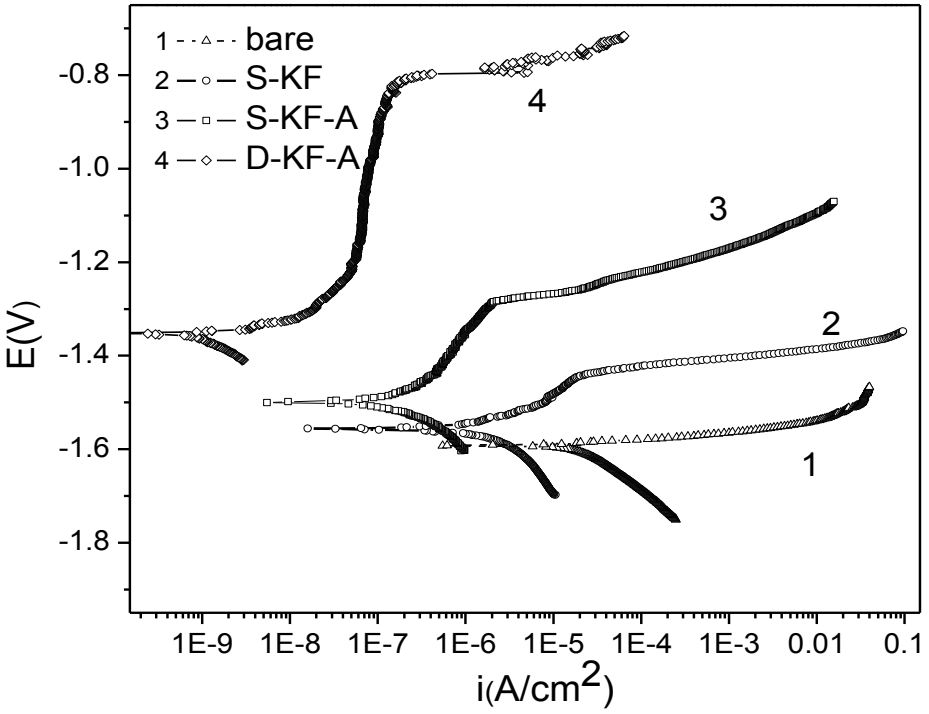

Figure 5. Potentiodynamic polarization curves of Mg alloy AZ91D with and without PEO coatings in 3.5% NaCl solution for10 h immersion.

Table 2. Parameters of potentiodynamic polarization curves of PEO coatings on Mg alloy AZ91D immersed in 3.5% NaCl solution for 10 h.

Immersion time	Samples	E_{corr}(V)	i_{corr}(A/cm^2)	βa(mV)	Rp(Ω cm^2)	F
10h	Bare	-1.5967	2.2696E-4	27.883	1.1494E2	
	F-M	-1.5670	1.5493E-6	60.890	2.5180E4	0.039
	F-M-A	-1.5063	3.0734E-7	72.223	1.1063E5	5.944×10-5
	F-B-A	-1.3715	1.2969E-9	102.54	3.1123E7	3.096×10-12

3.5 EIS characteristics

In order to understand better the corrosion performance, EIS measurement of F-B-A ceramic coating/magnesium alloy was conducted in 3.5%wt NaCl solution for a long-term.

Fig.6 represents the evolution of impedance diagrams for F-B-A coating in the 3.5% NaCl solution with immersion time. Taking into account these typical EIS plots, special morphology of F-B-A coating, as well as the relevant results in references [31-33], three equivalent circuits for Mg alloy electrode with F-B-A coating were proposed in Fig. 7(a) ~ (c).

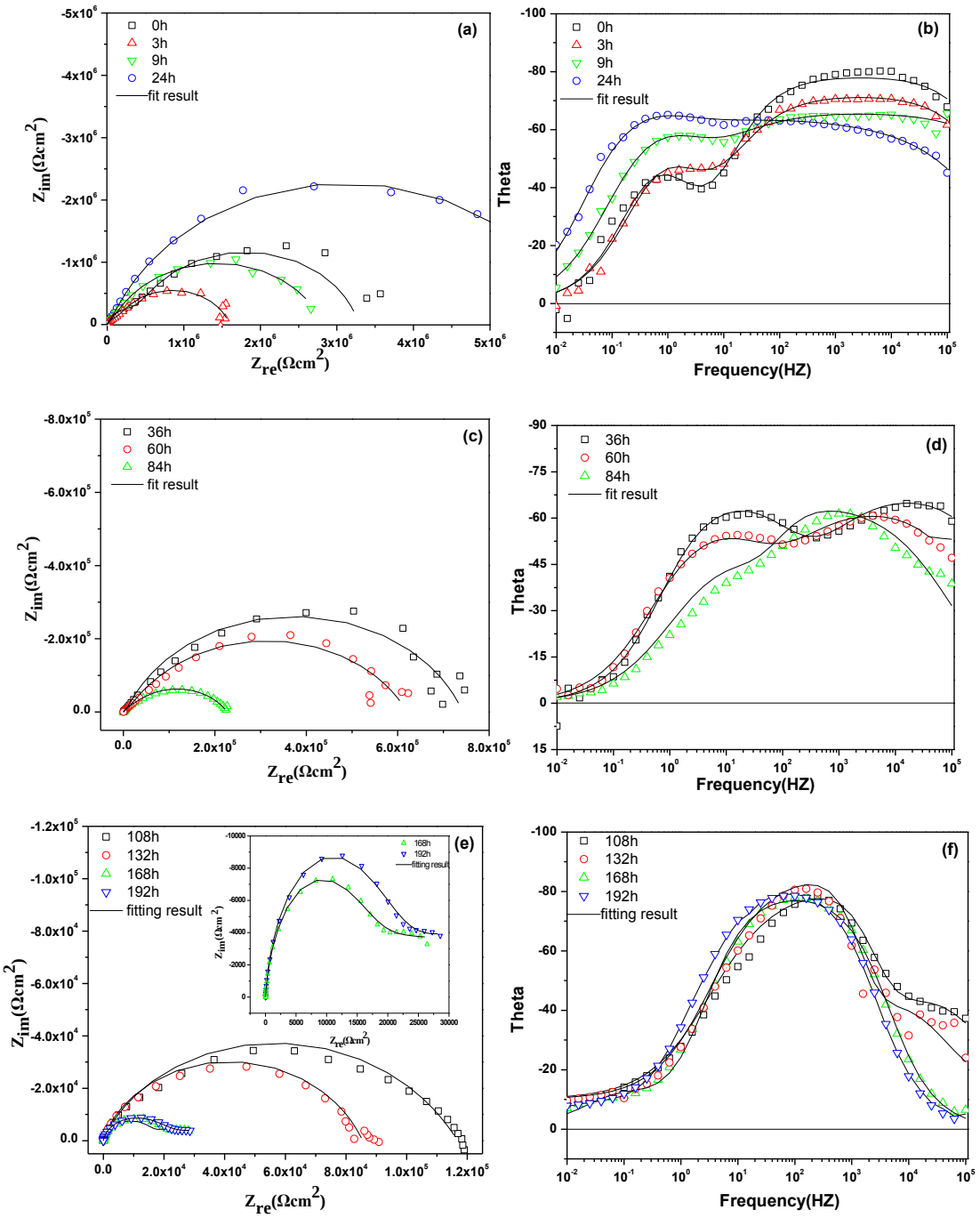

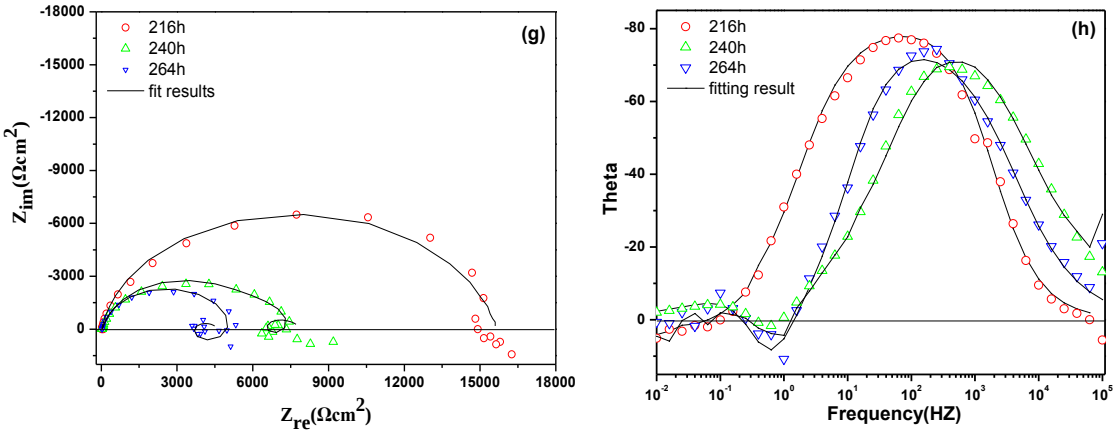

Figure 6. Nyquist and Bode diagrams for Mg alloy with F-B-A coating in 3.5% NaCl solution for different immersion time

During the initial stage of immersion (0~132h), the outer layer and the inner barrier layer of B-F-A coating both were low porosity, and corrosion cells at the mental/coating interface would be uniformly distributed, so, the equivalent circuit model of Fig. 7(a) will be fitted.

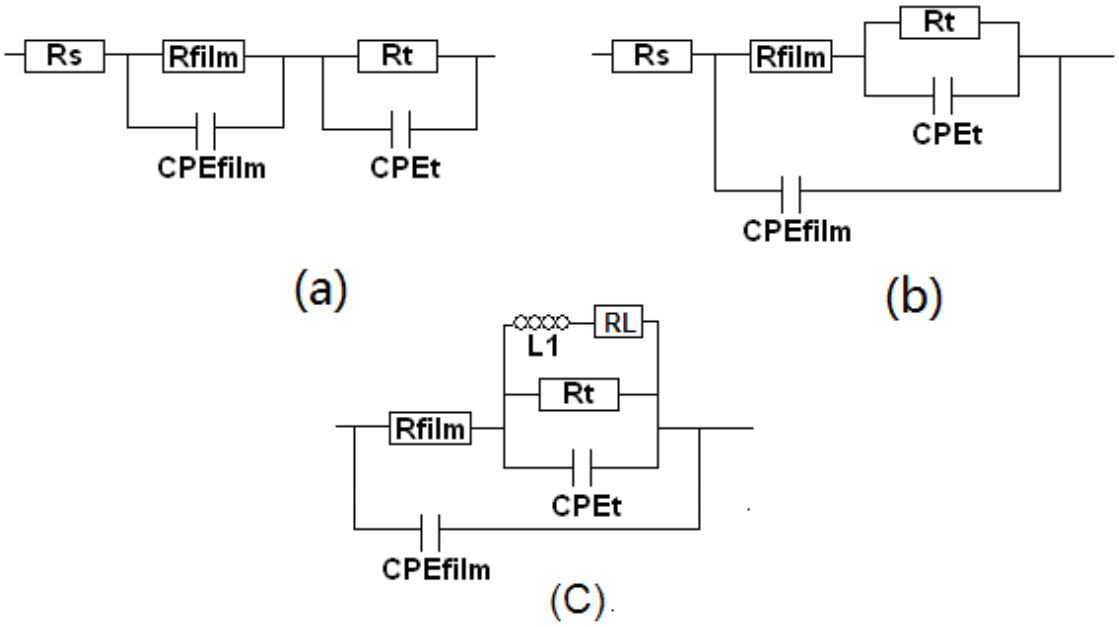

Figure 7. Equivalent circuits used for impedance data fitting of Mg alloy with F-B-A coating immersed in 3.5% NaCl solution.

However, with increasing immersion time, defects or micro-pore began to initiate in PEO coating, therewith, electrochemical reaction at the interface mental/coating would occur locally ,thus the equivalent circuit model of Fig. 7(b) was used to describe changes of impendence diagrams in that period. In addition, when the pitting corrosion occurred on the surface of PEO coating, as shown in

Fig.7(c), an inductor L and a R_L,were added to the electrical equivalent circuit model, parallel with the equivalent circuit (Rt,CPEt), representing the formation, adsorption and desorption of the corrosion products on the surface of electrode[23,31-32]. By the equivalent circuits, these EIS curves were best fitted as solid lines passing through the testing data (Fig.6). The corresponding values of the equivalent elements were listed in Table 3. From Fig.6 and Table 3, it can be seen that the impedance plots and the fitting results illustrated clearly the deterioration processes of the F-B-A coatings in long-term immersion tests.

Table 3. Fitting results of EIS plots of Mg alloy with F-B-A coating based on the equivalent circuit

Immersion time (h)	The F-B-A coating on AZ91D magnesium					
	R_{film}(Ω.cm^2)	CPE_{film}(F/ cm^2)	n_1(0-1)	R_t (Ω.cm^2)	CPE_t(F/ cm^2)	n_2(0-1)
0h	3.6929e5	6.0850e-8	0.879	2.9172e6	2.8345e-7	0.852
3h	1.3428e5	2.3046e-7	0.796	1.4623e6	5.0869e-7	0.816
9h	80328	1.0520e-6	0.695	2.7599e6	5.8971e-7	0.788
24h	57180	2.8652e-6	0.609	6.1308e6	5.8682e-7	0.809
36h	32563	6.3555e-7	0.701	6.0378e5	5.4353e-7	0.804
60h	17868	7.0538e-7	0.728	6.1103e5	7.0485e-7	0.721
84h	12083	4.6059e-7	0.875	2.1405e5	1.1615e-7	0.676
108h	9835	1.1056e-6	0.682	1.1595e5	6.7872e-8	1.003
132h	5570	1.1339e-6	0.704	84809	2.0543e-7	0.981
168h	724.9	4.8303e-6	0.905	9890	1.984e-4	0.773
192h	579.6	1.1339e-6	0.704	11289	2.0543e-7	0.981
216h	3800	9.1855e-6	0.909	5570	1.263e-5	1.074
240h	4626	8.424E-5	0.647	3808/858	3.989E-6	0.959
264h	4611	1.652E-5	0.691	3319/887	1.866E-6	0.981

In the initial period 0~24 h of immersion, Bode phase angle diagrams presented in Fig.6(b) show that two time constants were clearly distinguished in the high to medium frequencies domain, i.e. from10^4 Hz to10^{-1}Hz. It should reflect the performance of the dense outer layer (HF part) and the inner barrier layer (LF part), respectively [31]. The phase angle maximum for the HF part decreased with immersion time, whereas the phase angle for the LF frequency part gradually increased. The fitting result (in Table 3) showed that the Rfilm value, which presented the resistance of the dense outer layer, decreased from 3.6929e5Ω/cm2 to 57180Ω/cm2 during the initial period 0~24 h. However, the Rt value, which presented the resistance of the barrier layer at the mental/coating interface, decreased firstly and then increased after 3h immersion from 1.4623e6Ω.cm^2 to 6.1308e6Ω.cm^2.

The major event occurred in this period was the water/chloride ion infiltrating into the film, which gradually filled the pores of the coating. However, due to the compact nature of the barrier layer, aggressive electrolyte could not permeate the coating as easily as water molecules [34, 35], whilst the following reactions could occur in the barrier layer:

$$MgO+H_2O=Mg(OH)_2 \quad (1)$$

$$Mg+2H_2O=Mg(OH)_2+H_2 \quad (2)$$

The formation of oxidation products could lower the ionic dissolution rate of the metal , which resulted in a significant increase of R_t during the period of 3~24 h. However, the accumulation of corrosion products will give rise to stress in the barrier layer. A volume expansion of the barrier layer may be expected due to transformation of unstable compound MgO into $Mg(OH)_2$[36].Therefore, micro-cracks inside the barrier layer may be induced ,which will accelerate the migration rate of aggressive medium through the barrier layer. Thus, as shown in Table.3, the resistance of the coating (R_t) begin to decline gradually after 24 h.

Fig.8(a) and Fig.9(a) show the surface and cross-sectional morphology of PEO coating after immersed in NaCl solution for 24 h, it can be seen that the F-B-A coating kept intact and the outer layer of PEO coating was still compact, especially, the inner barrier layer kept well adhesive to the substrate. In other words, no obvious corrosion damage occurred in F-B-A coating or substrate within this period.

During 36~84 h immersion, the maximum phase angle corresponding to the two constants in the Bode plot (Fig.6(d)), shifted to a lower frequency, and the diameter of the corresponding capacitive loop in the Nyquist plot (Fig.6(c)) decreased slowly. As shown in Table.3, R_{film} and R_t, decreased gradually. In general, water molecule and corrosive species would be picked up by pores and cracks of the coating, thereby, the formation of conductive paths in the coating might decrease its dielectric characteristics (R_{film}), moreover, the aggressive ion penetrating through cracks and holes up to the interface may induce directly corrosion of the metal surface, so, R_t would decrease subsequently. From Fig.8 (b) and Fig.10 (b), it can be seen that the amount of micro-pores and micro-cracks in the F-B-A coating after 84 h immersion seemed higher than those of PEO coating immersed for 24 h. But, no signs for pores or flaws, which passed through the coating, were found, especially, no corrosion product at the coating/substrate interface should be detected. It implied that in this stage, although being filled gradually with electric media, nevertheless, the F-B-A coating was still in a good condition.

After immersed in 3.5%NaCl for 108~192 h, Fig.6(f) showed that the two main phase angles disappeared gradually and only one maximal phase angle existed at frequency 103 HZ in the Bode plot. However, in Nyquist plots, besides a depress capacitance loop in the mid-high frequencies, a new loop appeared in LF part after immersion for 168h, which was generally [37~38] owed to the mass transportation in solid phase, i.e. to the diffusion of ions through the oxide scale on metal surface. The fitting data showed that (Table 3), here, the resistance of the coating, R_{film}, declined significantly from $9835\Omega.cm^2$ to $579.6\Omega.cm^2$. Nevertheless, the barrier layer still maintained a high resistance, $11289\Omega cm^2$; this implies that the barrier layer may remain intact.

Fig.8(c) shows clearly a pore on the surface of PEO coating. However, EDS results at the bottom of that pore (Fig.9 (a)) did not reveal obviously peak of O, which related to the corrosion products (MgO or $Mg(OH)_2$), moreover, the peak representing Cl^- was also not detected. The facts suggested that the pore formed on the surface of F-B-A coating might not pass through up to the substrate. The cross-sectional morphology (Fig.10(c)) also showed that some corrosion products were

formed beneath the inner barrier layer of PEO coating, however, the barrier layer itself kept intact and did not damaged due to internal stress produced by this corrosion products.

Obviously, with the penetration of corrosive media, the unstable MgO in F-B-A coating might gradually dissolve and the $KMgF_3$ phase also transform into MgF_2 by reaction with accumulated H^+ ion into defects of the coating, eventually, the outer layer of F-B-A coating might badly be damaged, and as a result, many defects (big pores, deep cracks,) might develop on the surface. Thus, considering the high conductivity of the electrolyte inside big pores, the resistance of the porous layer became too small to be detected by impedance measurement (Fig. 6(f)). However, the inner dense layer adhered so tightly to the substrate, although Mg substrate beneath the barrier layer might be deteriorated gradually by the permeated aggressive ions, the formed corrosion products would mainly be intruded into micro-defects nearby the barrier layer, inducing the so called "pore block" (Fig. 10(c)), which would retard greatly the mass transportation process in the coating. This process was represented by finite length diffusion in LF par of the capacitive loop in Nyquist plot (Fig.6(c)). Therefore, during this period (108~192 h), as a second protective layer, the inner barrier layer of F-B-A coating could still prevent the substrate from Cl^- ion attack.

After 216 h immersion, the capacitive loop in Nyquist plot sharply shrinked (Fig.6 (g)). At the same time, R_t in table 5, representing the resistance of inner layer, decreased sharply to 5570 Ω/cm^2. As shown in Fig.8 (d), a larger and deep pit appeared on the surface of PEO coating, and EDS analysis (Fig.9 (b)) revealed a high peak of O which might mainly be the result of the formed corrosion products (MgO and $Mg(OH)_2$); also, a distinct peak of Cl from corrosive media was detected. The facts should be related with that the pitting-corrosion products might partially come from the substrate beneath the bottom of pore. From the Fig. 10(d), it showed that the coating was locally and intensively damaged with corrosion products penetrating depth into the substrate, as well as piling up on top of the outer surface of the sample. It indicated that after 216 h, enough corrosive electrolytes might pass through the coating up to the substrate; subsequently, the corrosion products (magnesium hydroxide) formed and accumulated extensively at the interface so that to exert stresses to damage the PEO coating.

In the next period of 240~264 h immersion, a depressed capacitance loop with an inductive loop distinctly appeared in the Nyquist plot (Fig.6(g)).The inductive loop usually demonstrated the formation and adsorption of corrosion products on active sites of the metal surface[39]. The equivalent circuit in Fig.8(c) was employed to fit the impedance spectra after pitting corrosion. According to Table 3, R_{film}, representing the resistance of pores in the coating, showed an increasing tendency, while Rt continuously decreased. The fact was that, with the pit growing into the substrate, the final corrosion products (MgO and $Mg(OH)_2$) were piled up and plugged into pores and cracks of the coating[40,41], which might enhance the corrosion resistance of the coating to a certain extant. However, the high concentration of chlorine ion accumulated at the interface region and then accelerated the pitting corrosion of the substrate alloy. The surface morphology of F-B-A coating (Fig.8 (e)) showed that the entire surface was rapidly covered with corrosion products, which mainly consisted of Mg, O and Cl according to EDS analysis (Fig.9(c)). Besides, Fig.10(e) showed that the whole PEO coating was destroyed heavily by the massive corrosion products from Mg substrate and

these corrosion products have spread over the top surface of PEO coating, i.e. the F-B-A coating completely lose its protectiveness.

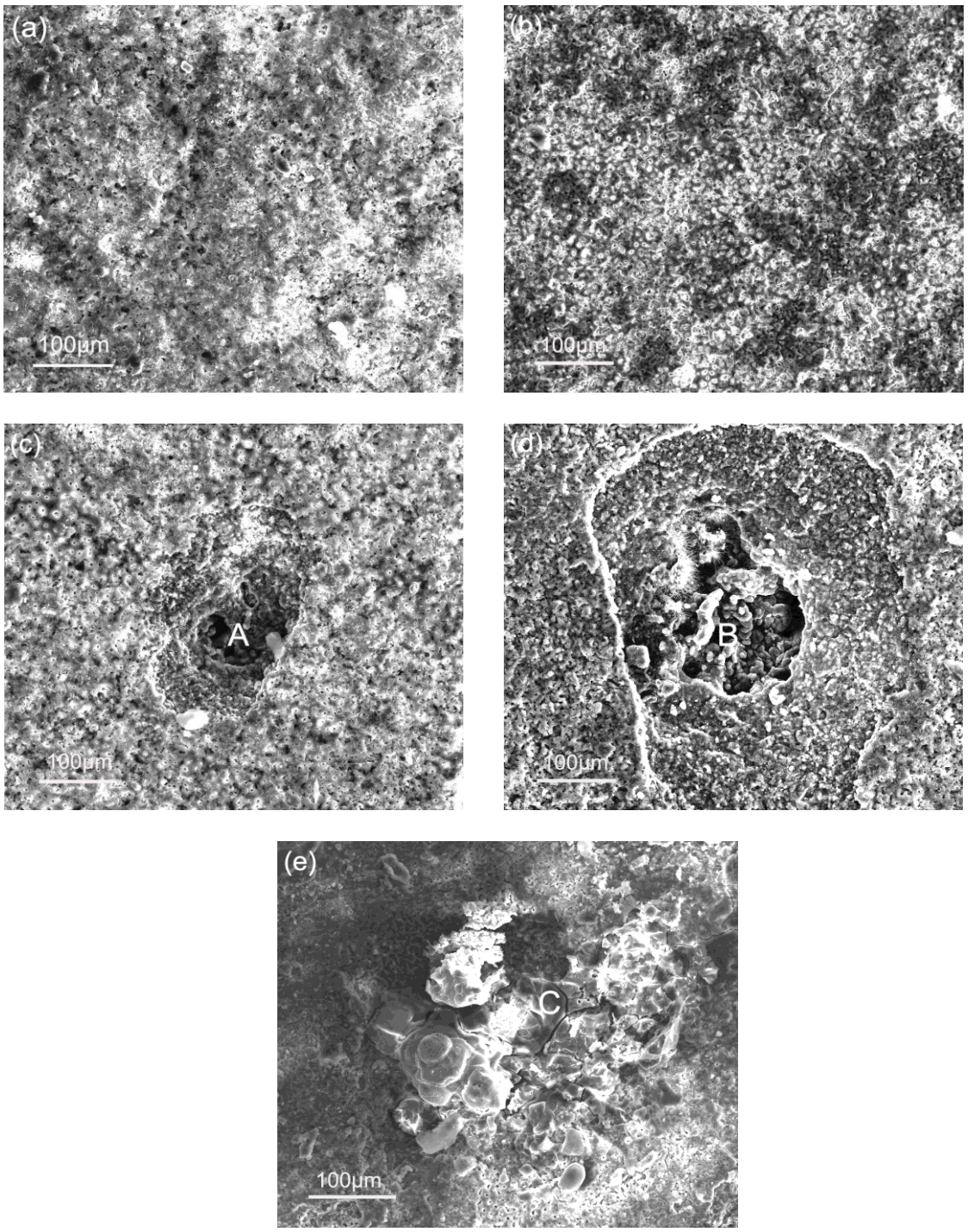

Figure 8. SEM of the surface of the AZ91D alloy with F-B-A coating when immersed in 3.5% NaCl solution for different time. (a)24h;(b)84h;(c)168h;(d)216h; (e) 264h

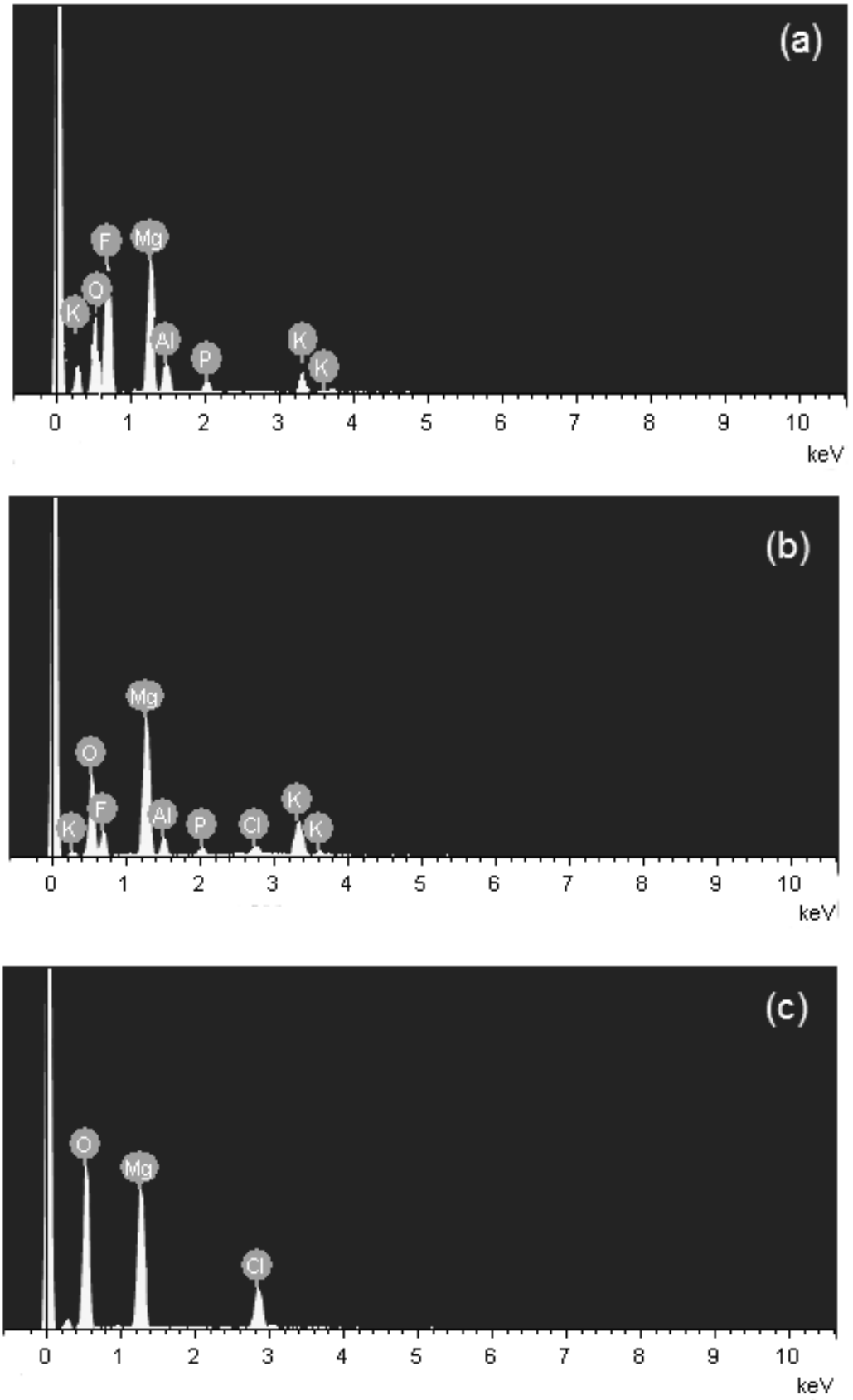

Figure 9. EDS spectra of (a) F-B-A coating (section A in Fig. 8c) and (b) F-B-A coating (section B in Fig. 8d) and (c) F-B-A coating (section C in Fig. 8e) on magnesium alloy AZ91D.

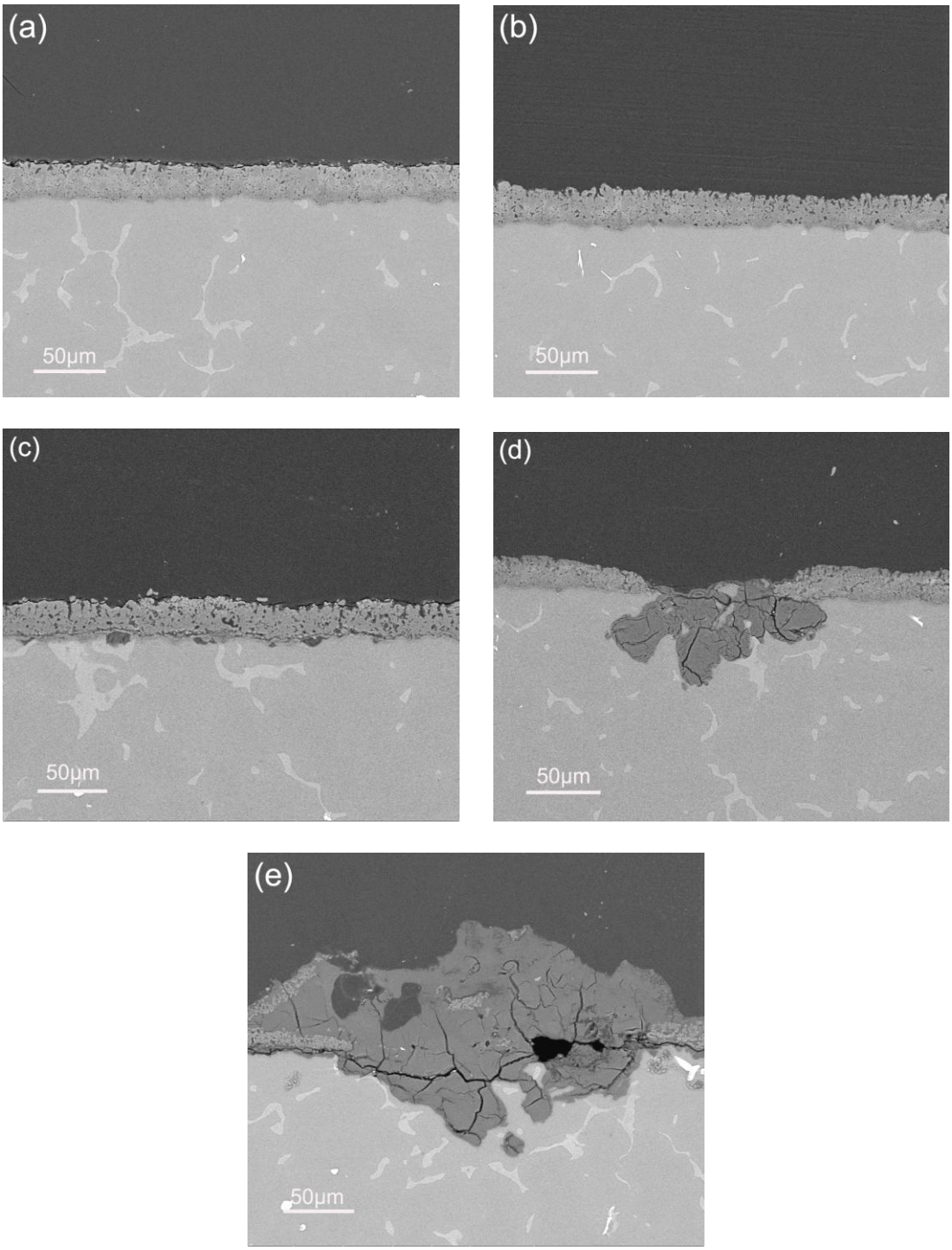

Figure 10. SEM of the cross-section of the AZ91D alloy with F-B-A coating when immersed in 3.5% NaCl solution for different time (a)24h;(b)84h;(c)168h;(d)216h; (e) 264h.

4. CONCLUSIONS

Three PEO ceramic coatings with different microstructure have been prepared on Mg alloy AZ91D in KF based electrolyte by different processing parameters. By applying voltage in a mono-

polar mode, the F-M coating prepared in blank KF electrolyte was most loose and porous; and after addition of phosphate into the base electrolyte, the F-M-A coating with a relative denser barrier layer was formed on Mg substrate; while the F-B-A coating prepared in the KF based electrolyte with additive by applying voltage in a bipolar mode exhibited a bi-layered and well compact morphology. Phases $KMgF_3$ and MgF_2 were the dominated constituents of F-B-A coating and peculiarly the inner barrier layer of F-B-A coating was mainly consisted of stable compounds such as MgF_2, $Mg_3(PO_4)_2$ and $MgHPO_4$.

Potentiodynamic polarization results indicated that the F-B-A coating provided the best corrosion protection for the substrate among the three coatings. Its corrosion current was three orders lower and its corrosion potential was 200mV higher than that of the poorest coating. EIS data indicated that the F-B-A coating possessed superior corrosion resistance in 3.5% NaCl solution for long-term; however, pitting corrosion and obvious corrosion products occurred on the surface of F-B-A coating after 216 h immersion. The outer layer with low porosity and a dense barrier layer without any defects in F-B-A coatings consisted of stable constituents, such as, MgF_2, $Mg_3(PO4)_2$ and $MgHPO_4$ were the key factor for delaying the substrate alloy to be corroded by corrosive media.

It can be concluded that in the noble acidic KF system, both the addition of phosphate and the application of bi-polar pulse voltage played an important role in preparation of PEO coating on Mg alloy AZ91D with compact structure and excellent corrosion resistance.

ACKNOWLEDGEMENT

This work was supported by project supported by National Science and Technology Ministry (Grant No.2011BAE22B05), Material foundation and application technology of key projects(Grant No. A0920110028) and the National Natural Science Funds (Grant No.51001107).

References

1. G.L. Song, Z.M. Shi, A. Atrens, *Corros. Sci*. 48 (2006) 1939.
2. L.J. Zhang, J.J. Fan, Z. Zhang, F.H. Cao, J.Q. Zhang, et al., *Electrochim. Acta*. 52 (2007) 5325.
3. L.O. Snizhko, A.L. Yerokhin, A. Pilkington, N.L. Gurevina, D.O. Misnyankin, A. Leyland, A. Matthew. *Electrochim. Acta*. 49 (2004) 2085.
4. F. Chen, H. Zhou, B. Yao, et al. *Surf. Coat Technol*. 201 (2007) 4905.
5. Q.Z. Cai, L.S. Wang, B.K. Wei, et al. *Surf. Coat Technol*. 200 (2006) 3727.
6. S.J. Xia, R. Yue, Jr. R.G. Rateick, et al. *J. Electrochem. Soc*. 151 (2004) B179.
7. D. Y. Hwang, Y. M. Kima, D.-Y. Parkb, B.Y.Yoo, D.H. Shina, *Electrochim. Acta.* 54 (2009) 5479.
8. S.V. Gnedenkov, O.A. Khrisanfova, et al., *Surf. Coat Technol*. 204 (2010) 2316.
9. H.P. Duan, C.W. Yan, F.H.Wang. *Electrochim. Acta*.52 (2007) 3785.
10. J. Liang, B. Guo, J.Tian, et al., *Appl.Surf.Sci*.252 (2005)345.
11. H.-Y. Hsiao, H.-C. Tsung,W.-T.Tsai, *Surf.Coat.Technol*.199(2005)127.
12. L.Wang. L.Chen.Z.Yan.H.Wang.J.Peng. *J.Alloy.Comp*.480(2009)46.
13. H. Luo, Q Cai, B. Wei, et al. *J. Alloy Comp*. 464 (2008) 537.
14. J. Liang, P.B. Srinivasan, C. Blawert, et al. *Electrochim. Acta*. 54 (2009) 3842.
15. A.V. Timoshenko, Yu. V. Magurova. *Surf.Coat.Technol*. 199(2005) 135.

16. V.Brass, S.Xia, R.Yue, G.Richard, Rateick Jr. *J.Electrochem.Soc*.151(2004) B1.
17. S.V.Gnedenkov,O.A.Khrisanfova,A.G.Zavidnaya,et al.*Surf.Coat.Technol*. 204(2010)2316.
18. G.Antou, G.Montavon, Franc, oise Hlawka, et al., *Surf.Coat.Technol*. 627 (2004)180.
19. G. Antou ,F. Hlawka , A. Cornet ,C. Becker , et al., *Surf. Coat. Technol*. 200 (2006) 6062.
20. C.Liu, Q.Bi, A.Leyland, A.Matthews, *Sci.Forum* 44-45(1989)29.
21. B. Matthes, E. Broszeit, J. Aromaa, H. Ronkainen, S.P.Hannula, A. Leyland, A. Matthews, *Surf. Coat. Technol*. 49(1991) 489.
22. A.Ghasemi,V.S.Raja.C.Blawert,W.Dietzel,K.U.Kainer.*Surf.Coat.Technol*.202(2008)3513.
23. Z. Yao, Y. Lia, Y. Xu, Z. Jiang, F. Wang, *Mater. Chem. Phys*.126 (2011) 227.
24. X. Sun, Z. Jiang, Z. Yao, X. Zhang, *Appl. Surf. Sci*. 252 (2005) 441-447.
25. Lei Wang,Tadashi Shinoharaa,Bo-Ping Zhang, *Appl. Surf. Sci.* 256 (2010) 5807.
26. Houng-Yu Hsiao,Wen-Ta Tsai. *Surf.Coat.Technol*. 190(2005) 299.
27. W.Q. Zhou, D.Y. Shan, E.H. Han, *Corros. Sci.* 50(2008)329.
28. L. Kouisni, M. Azzi, M. Zertoubi, et al., *Surf.Coat.Technol*. 185(2004)58.
29. Wagner CD, Riggs WM, Davis LE, Moulder JE, Mulenger GE, Handbook of X-ray photoelectron spectroscopy Eden Prairie,MN:Perdin-Elmer Corp.,1979.
30. H.Chen,G.H. Lv,G.L.Zhang,et al. *Surf. Coat. Technol*. 205 (2010) 532.
31. J. Liang, P. Bala Srinivasan, C. Blawert, et.al. *Electrochim.Acta.* 54 (2009) 3842.
32. J. Liang, P. Bala Srinivasan, C. Blawert, et.al. *Electrochim.Acta.* 55 (2010) 6802.
33. J. Liang, L.T. Hu,J.C. Hao, *Appl.Surf.Sci*.253(2007)6939.
34. F. Mansfeld, *Electrochim. Acta*. 35 (1990) 1533.
35. V. Lopez, M.J. Bartolome, E. Esudero, et al. *J. Electrochem. Soc*. 153 (2006) B75.
36. H.P.Duan,K.Q. Du,et al ,*Electrochim.Acta.* 51(2006)2898-2908.
37. S.J.Xia.R.Yue.R.G.Rateick Jr.,V.J.Virss.*J.Electrochem.Soc*.151(3)(2004)B179.
38. G.G.Perrault, Electro. chem. inter. *Electro.* 51(1974)107.
39. K,Jütter,W.J.Lorenz,M.W.Kendig,et al.*J.Electrochem.Soc*.135(1988)332.
40. S.J.Xia.R.Yue.R.G.Rateick Jr, V.J.Virss, *J.Electrochem.Soc*.151 (2004) B179